Communication

Omnidirectional Dual-Polarized Saber Antenna With Low Wind Drag

Peiqin Liu, Zhijun Meng, Lifeng Wang, Yongjian Zhang, and Yue Li

***Abstract*— In this communication, a compact saber-like antenna with low wind drag is proposed for on-board communication application, under the requirements of polarization diversity and omnidirectional coverage. The proposed antenna consists of a thin resonant cavity for omnidirectional horizontal polarization (HP), and a folded slot is colocated with the cavity to provide omnidirectional vertical polarization (VP). Isolation lower than −20 dB between two feeding ports is achieved in a quite compact dimension of $30 \times 29 \times 9$ mm^3($0.24\lambda_0 \times 0.24\lambda_0 \times 0.07\lambda_0$, λ_0 is the free-space wavelength at 2.44 GHz), also with the omnidirectional patterns for both polarizations. A prototype of the proposed antenna is fabricated and tested to verify the design strategy. Compared with previous designs, the cross section area for wind drag is reduced for more than 28.5%, exhibiting potential usage for high-speed moving antenna carriers.**

***Index Terms*— Cavity antennas, low wind drag, polarization diversity, radiation patterns, saber-like structure.**

I. Introduction

In the past decades, dual-polarized antennas have attracted great attention due to polarization diversity [1]–[4]. Extensive researches about dual-polarized antennas have been carried out and adopted in wireless communication systems, such as spacecraft communication systems [5], [6], filtering antennas with high isolation [7], [8], and synthetic aperture radar (SAR) [9].

Omnidirectional antennas have the merit of 360° full coverage in the azimuthal plane [10], [11]. Omnidirectional radiation property is required in numerous wireless communication systems, such as wireless local area network (WLAN) [12], base stations [13], and portable devices [14]. Lot of researches are proposed to design dual-polarized antenna with omnidirectional radiation patterns. For omnidirectional dual-polarized antenna (ODPA) design, it is quite important to choose radiation elements for vertical polarization (VP) and horizontal polarization (HP). Dipole antennas are popular in designing single-polarized antenna. By locating orthogonal dipoles around a cylindrical structure, a dual-polarized omnidirectional antenna is proposed in [15]. Biconical antenna and discone antenna are widely used wideband antennas for omnidirectional VP. By combining them with dipole antennas, multiband and wideband dual-polarized omnidirectional antennas are achieved in [16]–[19]. Dielectric resonator antenna (DRA) is another design strategy to achieve ODPA with 3-D structure, which offers dual polarizations in one antenna volume [20]. Besides multiband and wideband dual-polarized designs, several researches are proposed to design dual-polarized omnidirectional with low-profile property. In [21], a circular patch is integrated with branches to achieve dual-polarized and omnidirectional radiation. In [22], slot antennas are combined with circular patch to design dual-band ODPA. Moreover, artificial magnetic conductor (AMC) is an effective technique to reduce the height of ODPAs, which makes a trade-off between bandwidth and low-profile property [23], [24].

Fig. 1. General scenario of the proposed antenna in aircraft applications.

Recently, several researches are proposed to design ODPAs in space-limited applications, such as communication systems between cars or aircrafts. As shown in Fig. 1, antennas in vehicles require a peculiar saber-like structure to reduce the wind drag. So that the antenna can be put inside an aerodynamic cover and reduce the wind drag [25]. In [26] and [27], a monopole antenna is colocated with a slot antenna to achieve dual-polarized for small-volume terminals. In [28] and [29], orthogonal slots are arranged on a slender columnar structure to improve the omnidirectional radiation property. However, the slender column structures still have a relatively large cross section in front area. It is a challenge to reduce the cross section area for vehicle communication applications.

For this purpose, in [30], we have proposed an ODPA with saber-like structure to reduce the wind drag without deteriorating the omnidirectional coverage property. A tilted monopole antenna is colocated with a cavity antenna to achieve dual-polarization and omnidirectional radiation in the azimuthal plane. However, the tilted monopole in [30] makes the overall structure's profile quite high and the achieved wind drag cannot fulfill the on-board requirements. In this communication, as a nontrivial improvement, we replace the tilted monopole with a folded slot, which is directly cut on the cavity body, without utilizing external structure as in [30]. Here, in this work, a thin resonant cavity antenna is used for omnidirectional HP. More importantly, by etching a folded slot on the middle of the cavity, the omnidirectional VP is achieved. In previous works, the radiators for HP and VP are arranged separately. In the proposed antenna, the slot is directly etched on the cavity. The two radiators are successfully integrated together owing to the orthogonal property between slot mode and cavity mode. As a result, the cross section

Manuscript received November 2, 2018; revised June 10, 2019; accepted July 29, 2019. Date of publication August 16, 2019; date of current version January 3, 2020. This work was supported in part by the National Natural Science Foundation of China under Contract 61771280 and in part by the Beijing Natural Science Foundation under Contract 4182029. *(Corresponding authors: Zhijun Meng; Yue Li.)*

P. Liu, Y. Zhang, and Y. Li are with the Department of Electronic Engineering, Tsinghua University, Beijing 100084, China (e-mail: lyee@tsinghua.edu.cn).

Z. Meng and L. Wang are with the School of Aeronautic Science and Engineering, Beijing University of Aeronautics and Astronautics, Beijing 100191, China (e-mail: mengzhijun@buaa.edu.cn).

Color versions of one or more of the figures in this communication are available online at http://ieeexplore.ieee.org.

Digital Object Identifier 10.1109/TAP.2019.2934566

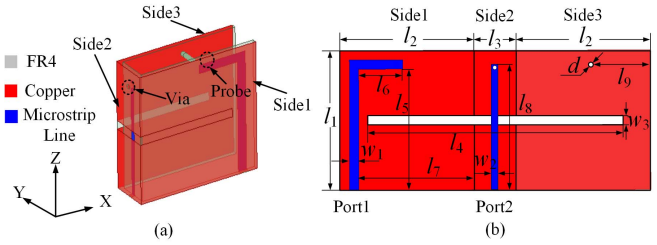

Fig. 2. Geometry of the proposed antenna. (a) Perspective view. (b) Expanded view.

TABLE I
OPTIMIZED DIMENSIONS (UNIT: mm)

Parameter	l_1	l_2	l_3	l_4
Value	30	29	9	55
Parameter	l_5	l_6	l_7	l_8
Value	26	9.5	25	27
Parameter	w_1	w_2	w_3	d
Value	2	1	2	1.1

area of the proposed antenna is reduced for more than 28.5%. The total volume of the new antenna is only $30 \times 29 \times 9$ mm^3($0.24\lambda_0 \times 0.24\lambda_0 \times 0.07\lambda_0$, λ_0 is the free-space wavelength at 2.44 GHz) and the cross section area is 30×29 mm^2($0.24\lambda_0 \times 0.24\lambda_0$). A prototype of the proposed antenna is fabricated and tested to validate the design strategy. The measured results are reported and discussed.

II. ANTENNA DESIGN

The geometry of the proposed saber-like ODPA is depicted in Fig. 2. The main structure of the antenna is a thin cavity for HP and a folded for VP. The folded slot is directly etched on the middle of the cavity, which can effectively reduce the profile for lower wind drag. As shown in Fig. 2, the red part is the copper, the gray part is the substrate, and the blue part is the feeding microstrip line. Fig. 2(a) is the perspective view. The thin cavity consists of three pieces of FR4 substrates ($\varepsilon_r = 4.4$, $\tan\delta = 0.01$), named as side1–side3. The thickness of the FR4 substrate is 1 mm. Fig. 2(b) shows the expanded view of the proposed antenna. The slot is parallel with the surface current in the cavity mode, such that the slot mode is with less effect to the cavity mode, achieving high isolation between two feeding ports. The cavity is fed through port 1. The microstrip line, which is connected with port 1, locates on side 1. At the end of the microstrip line, a probe connects the microstrip line with side 3 to excite the cavity mode. The slot is fed through port 2. The microstrip line for port 2 locates in the middle of side 2. At the end of the microstrip line, it is shorted by one via. The detailed parameters of the proposed antenna are listed in Table I.

A. Thin Cavity for Horizontal Polarization

In the previous design [30], a thin cavity is utilized to provide omnidirectional HP in the azimuthal plane. As discussed in [30], the operating frequency of the thin cavity is determined by the parameter l_1, and the feeding probe in [30] locates in the middle of the cavity. However, in this communication, the folded slot locates in the middle of the cavity for symmetry and high isolation. So, in the proposed antenna, the position of the probe should be tuned.

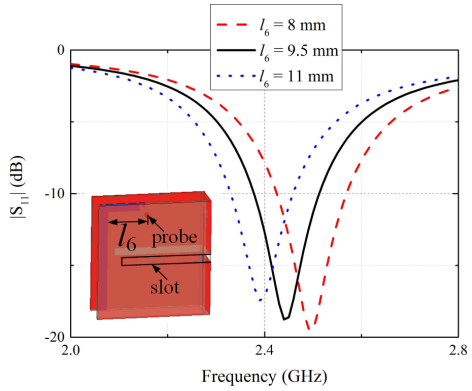

Fig. 3. $|S_{11}|$ of the proposed antenna with different values of l_6. Inset: Perspective view of the proposed antenna.

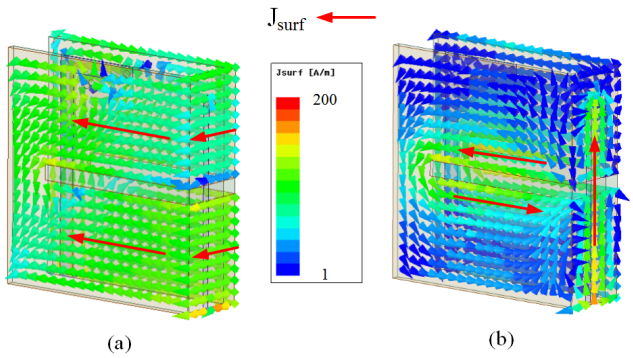

Fig. 4. Current magnitude distribution of the proposed antenna at 2.44 GHz. (a) Cavity mode. (b) Slot mode.

As shown in Fig. 2, the length of l_2 is about a quarter of λ_0, and the thin cavity operates in TE_{mnp} mode (m = 0.5, n = 0, p = 0), which means the electromagnetic field is almost uniform along z-axis and operates a quarter wavelength mode along x-axis. As a result, the probe can be moved along z-axis to the edge of the cavity without disturbing the operating mode of the cavity mode. Moreover, the parameter l_6, which represents the position of the probe in x-axis, determines the impedance match of the thin cavity. Fig. 3 shows the simulated $|S_{11}|$ results with different values of l_6. As l_6 increases from 8 to 11 mm, the operating frequency of the resonant cavity decreases. The bandwidth of the cavity is associated with the Q factor, which can be tuned by the dimensions of the cavity. Similar to the analyses in [30], the bandwidth of the thin cavity increases when l_1 increases. As a result, the parameter l_1 is optimized as a tradeoff between bandwidth and size miniaturization.

B. Slot for Vertical Polarization

For VP, the slot is directly cut on the cavity instead of in the external of the cavity, which contributes to reducing the height and wind drag of the antenna. Moreover, the slot is folded to achieve omnidirectional radiation. Fig. 4 illustrates the current magnitude distribution of the proposed antenna at 2.44 GHz. Fig. 4(a) is the current distribution of the cavity mode. Because the thin cavity operates in TE_{mnp} mode (m = 0.5, n = 0, p = 0), the vector surface currents are in phase and with the same direction. Considering that the slot is etched along the direction of the surface current in the cavity mode, the slot would not disturb the cavity mode. Fig. 4(b) shows the current distribution of the folded slot mode. For this mode,

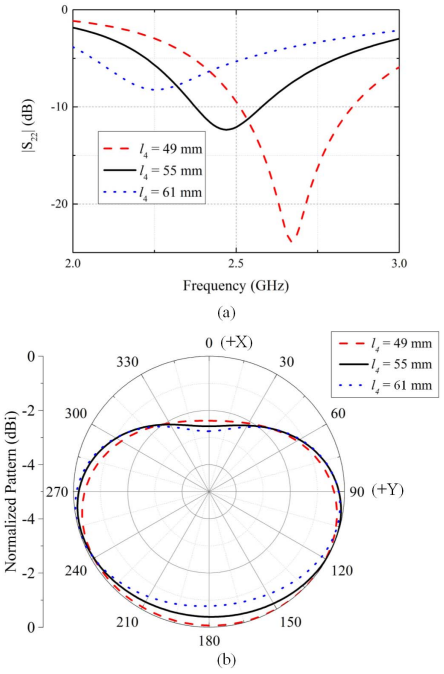

Fig. 5. Simulated results of the slot antenna with different values of l4. (a) $|S_{22}|$ of the proposed antenna with different values of l4. (b) Normalized radiation patterns for HP in the azimuthal plane at 2.44 GHz.

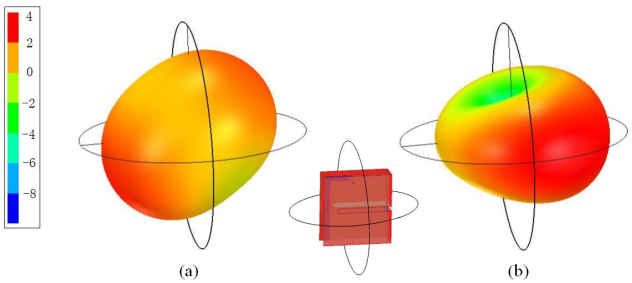

Fig. 6. Simulated 3-D radiation patterns of the proposed antenna at 2.44 GHz. (a) Cavity mode. (b) Slot mode.

one can observe that the currents around the slot are out of phase, contributing to the high isolation.

The parameter l_4 represents the length of the slot. The whole length of the slot is about $0.5\lambda_0$ and the slot operates in half wavelength mode. Fig. 5 shows the simulated results of the proposed antenna with different values of l_4. Fig. 5(a) shows the simulated $|S_{22}|$. Considering the half wavelength mode of slot, the operating frequency increases as the parameter l_4 decreases. Fig. 5(b) shows the normalized radiation patterns in the azimuthal plane at 2.44 GHz. When l_4 increases from 49 to 61 mm, the gain variations (the difference between the maximum gain and the minimum gain) increases from 2.38 to 2.77 dB, which is a slight variation and acceptable for application. The bandwidth of the slot antenna is determined by the width w_3. When the width increases, the bandwidth increases as well. However, if the width increases too much, the slot disturbs the cavity mode and the isolation between the slot mode and cavity mode degrades. So the parameter w_3 is optimized as 2 mm for an acceptable bandwidth.

The 3-D radiation patterns of the proposed ODPA at 2.44 GHz are illustrated in Fig. 6. Fig. 6(a) shows the 3-D pattern of the cavity mode (port 1). One can observe that the radiation pattern is almost

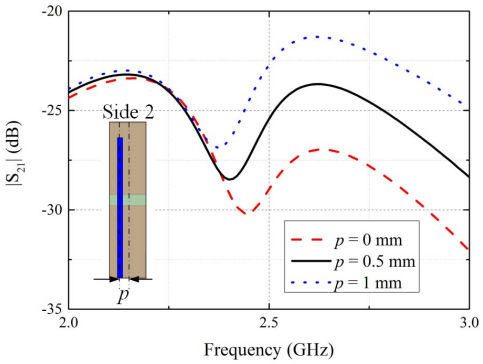

Fig. 7. Simulated $|S_{21}|$ results of the proposed antenna with different values of parameter p. Inset: Position of the feeding microstrip line for the slot antenna.

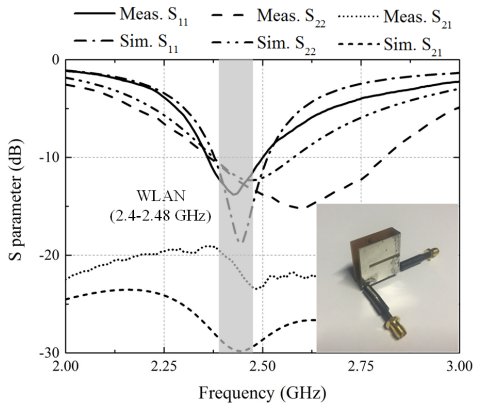

Fig. 8. Simulated and measured S-parameters of the proposed antenna.

uniform in the free space. In the azimuthal plane, the radiation pattern is omnidirectional and the gain variation (the difference between the maximum gain and the minimum gain) is 2.05 dB. Fig. 6(b) shows the 3-D pattern of the folded slot mode (port 2). The radiation pattern of the folded slot is with donut shape. The folded slot is on the right side of the cavity, and the gain in the right side is slightly stronger than the left side. The gain variation in the azimuthal is 2.58 dB, which is acceptable for practical applications.

The isolation between feeding ports is another key property for dual-polarized antennas. Fig. 4 illustrates that the cavity mode and the slot mode are orthogonal, which means there is potential to achieve high isolation. Fig. 7 shows the simulated $|S_{21}|$ results with different values of parameter p. As shown in Fig. 7, parameter p represents the position of the feeding microstrip line for port 2. When $p = 0$ mm, the microstrip line locates in the middle of side 2. As p increases, the microstrip line moves away from the middle line. When $p = 0$ mm, the proposed antenna achieves the best isolation between two ports. As p increases, the symmetry of the feeding structure is affected, causing the isolation deteriorates.

III. Measurement Results

A prototype of the proposed saber ODPA is fabricated and tested to verify the design strategy. The photograph of the proposed antenna is inserted in Fig. 8. Ferrite rings are used to prevent surface current on the feeding coaxial cables. In practical applications, the proposed antenna can be excited by a WLAN module, such as TiWi-C-W [31]. The module is implemented inside the cavity without the bulky coaxial cables and ferrite rings. The simulated and measured S

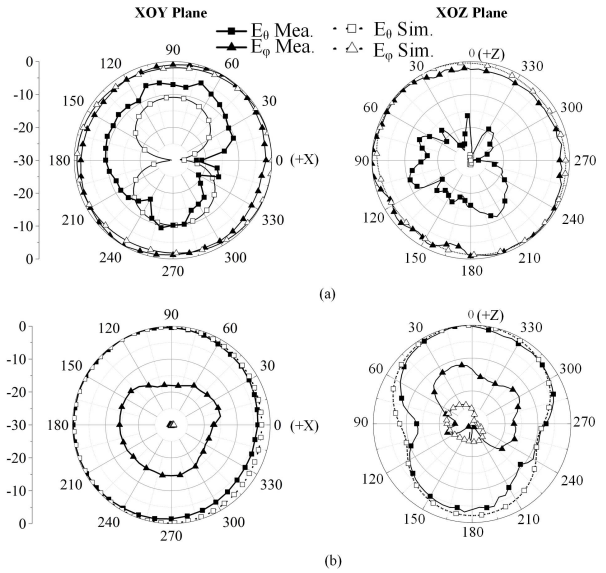

Fig. 9. Normalized radiation patterns of the proposed antenna at 2.44 GHz. (a) Port 1 (cavity mode). (b) Port 2 (slot mode).

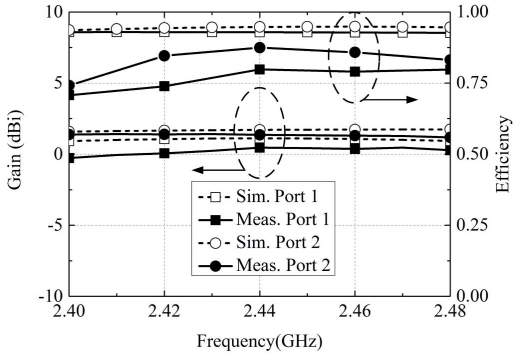

Fig. 10. Gain and efficiency of the proposed antenna.

TABLE II
QUALITY COMPARISONS

Ref.	Gain Variation (HP)	Gain Variation (VP)	Cross section area in front
[15]	1.5 dB	0.5 dB	$0.51\lambda_0\times0.67\lambda_0$
[16]	1.5 dB	1.5 dB	$1.54\lambda_0\times0.85\lambda_0$
[17]	3.3 dB	2 dB	$1.04\lambda_0\times1.04\lambda_0$
[28]	2.1 dB	2.9 dB	$0.67\lambda_0\times0.09\lambda_0$
[29]	2.4 dB	4.5 dB	$0.34\lambda_0\times0.10\lambda_0$
[30]	3.45 dB	3.60 dB	$0.34\lambda_0\times0.07\lambda_0$
This work	3.18 dB	4.41 dB	$0.24\lambda_0\times0.07\lambda_0$*

* All of the antennas are compared in free space without ground plane. In section IV, the proposed antenna is mounted above a circular AMC structure. The diameter of the AMC is $1.3\lambda_0$, and the thickness is $0.04\lambda_0$.

parameters of the proposed antenna are depicted in Fig. 8. The measured −10 dB bandwidth of the port 1 (HP) is 2.36–2.5 GHz. The measured −10 dB bandwidth of port 2 (VP) is 2.36–2.8 GHz. Both HP and VP meet the requirement of 2.4 GHz WALN application. The measured isolation is higher than 20 dB in the operating frequency. Compared with the simulated results, there are several discrepancies in the measured results. The measured −10 dB bandwidth of port 2 is wider than the simulated results, and the measured $|S_{21}|$ is higher than the simulated results. The discrepancies are attributed to fabrication errors.

The simulated and measured radiation patterns of the proposed antenna are illustrated in Fig. 9. The patterns are obtained in both the XOY plane and XOZ plane. The patterns in the XOY plane show the omnidirectional radiation property. Fig. 9(a) shows the normalized patterns for port 1 (cavity mode). In the simulated results, the gain variation in the XOY plane is 2.05 dB. For the measurement results, the gain variation is 3.18 dB. Fig. 9(b) shows the normalized patterns for port 2 (slot mode). In the simulated results, the gain variation for VP is 2.58 dB. For the measurement results, the gain variation is 4.41 dB, and it is still acceptable for practical applications. Fig. 9 also shows that the simulated cross polarization is less than −11 dB for port 1 and less than −29 dB for port 2. While the measured cross polarization is larger than simulation. Considering the prototype is manually fabricated and soldered, the discrepancies between simulated patterns and measured patterns are due to the fabrication errors. Moreover, using the feeding cables also degrades the radiation property. Fig. 10 shows the gain and radiation efficiency results of the proposed antenna. In the desired band of 2.4–2.48 GHz, the simulated gain of HP (port 1) is 0.91–1.11 dBi and −0.27–0.46 dBi for measurement. For the VP (port 2), the simulated gain is 1.58–1.74 dBi and 1.18–1.42 dBi for measurement. The measured results match well with the simulation. The simulated radiation efficiency is higher than 0.92 for both HP and VP. The measured efficiency decreases to about 0.8 in the center frequency. For the edge frequencies, the efficiency is about 0.75. The discrepancies are attributed to the fabrication errors.

According to [32], the signature of wind drag is a function of cross section, Cexpressed as $F_D = \rho v^2 C_D A/2$, where F_D is the drag force, ρ is the density of the fluid, v is the speed of the object relative to the fluid, A is the cross section in front, and C_D is the drag coefficient. So, large cross section area limits the applications in high-speed vehicles. Table II shows a comparison between the proposed antenna and previous researches. All the antennas provide omnidirectional radiation for both HP and VP in the azimuthal plane. The antennas in [15]–[17] have excellent omnidirectional radiation and broadband property. However, their dimensions are quite large and not suitable for space-limited applications. In [28]–[30], the antennas are designed with cylindrical or saber-like structures, which have small cross section area. Due to the size miniaturization, the omnidirectional property degrades. In this communication, the proposed antenna further reduces the cross section area by integrating a folded slot with a thin cavity. The cross section area of the proposed antenna is smaller than the antennas in [28]–[30] for 28.6%, 46.5%, and 70.5%, respectively. Also, the gain variations in the proposed antenna are still acceptable for practical applications.

IV. DUAL-POLARIZED ANTENNA WITH AMC STRUCTURE

For on-board applications, the proposed antenna would be implemented on metallic surfaces of the vehicles, but the pattern of HP is sharply deteriorated due to the metallic boundary condition, i.e., tangential electric fields are zero at metallic surface. To solve the problem, an AMC reflector is integrated with the proposed antenna. Considering that the width of the proposed antenna is relatively narrow, a miniaturized double-layer AMC structure [33] is utilized in this design. Fig. 11(a) illustrates the configuration with the AMC structure. The distance between the antenna and the AMC is only 5 mm, which is $0.04\lambda_0$ (λ_0 is the wavelength in free space

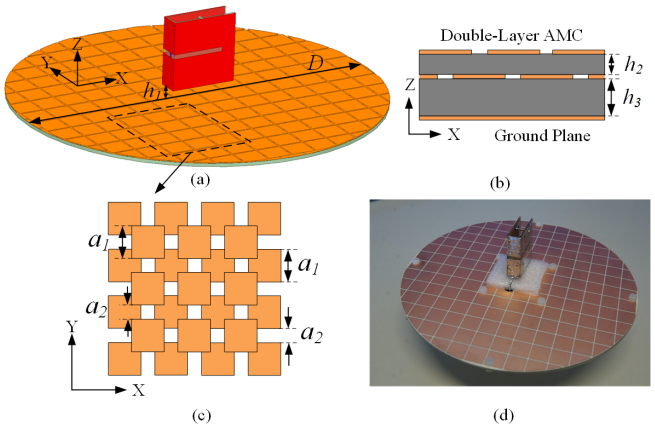

Fig. 11. Integrating the proposed antenna with AMC. (a) Configuration of the proposed antenna with AMC. (b) Side view of the double-layer AMC structure. (c) Front view of the double-layer AMC structure. (d) Photograph of the proposed antenna with AMC structure. Detailed dimensions of the AMC structure: $D = 160$ mm, $h_1 = 5$ mm, $h_2 = 0.508$ mm, $h_3 = 1.5$ mm, $a_1 = 10.5$ mm, $a_2 = 0.75$ mm.

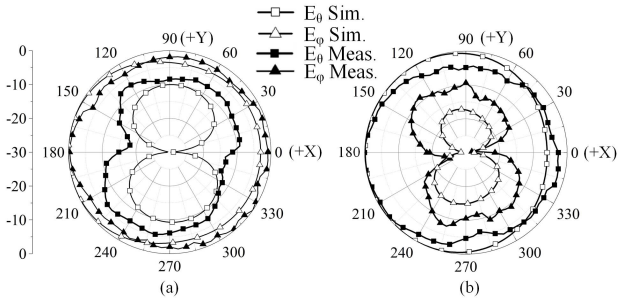

Fig. 12. Normalized patterns of the proposed antenna with AMC. (a) Patterns of port 1 (cavity mode) in the azimuthal (XOY) plane. (b) Patterns of port 2 (slot mode) in the azimuthal (XOY) plane.

at 2.44 GHz). Fig. 11(b) and (c) depicts the detailed dimensions of the double-layer AMC structure with the detailed parameters, which can be found in [33]. By utilizing the AMC structure, the proposed antenna can operate as a low wind drag antenna and be implemented with metallic surfaces. The AMC structure is fabricated to verify the design strategy. Fig. 11(d) shows the photograph of the proposed with the AMC structure.

The radiation patterns of the proposed antenna with the AMC structure are illustrated in Fig. 12. Fig. 12(a) shows the patterns of the cavity mode in the azimuthal plane at 2.44 GHz. For HP in the cavity mode, the gain variation in the simulated result is 3.7 dB, and the measured gain variation is 4.5 dB. Fig. 12(b) shows the normalized patterns of the slot mode in the azimuthal plane. For VP in the slot mode, the simulated gain variation is 5.8 dB and the measured gain variation is 6.3 dB. As shown in Fig. 11(d), the dual-layer AMC structure is manually bonded with screws instead of multilayer printed circuit board (PCB) process. As a result, there are some discrepancies in the measured results in radiation patterns. In practical applications, the errors can be eliminated by using standard PCB process. The results show that by using the AMC structure, the proposed antenna can be mounted on the surface of vehicles with a small distance and acceptable performance. Also, such deterioration would be mitigated by increasing the distance from the AMC surface with a tradeoff consideration.

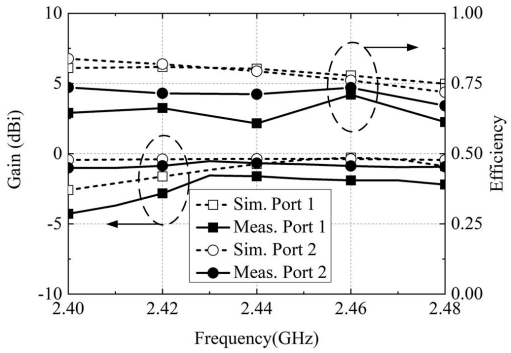

Fig. 13. Gain in the azimuthal plane and efficiency of the proposed antenna with AMC structure.

The gain and radiation efficiency of the proposed antenna with the AMC structure are depicted in Fig. 13. Owing to the AMC structure, the radiation patterns of the proposed antenna tilt upward. As a result, the gain in the azimuthal decreases. In the operating band of 2.4–2.48 GHz, the simulated gain of HP (port 1) is −2.58 to −0.29 dBi. In the measurement results, the gain is −4.28 to −1.55 dBi. For VP (port 2), the simulated gain is −0.45 to −0.36 dBi. In the measurement results, the gain is −1.01 to −0.53 dBi. It should be noted that the AMC structure has effects on radiation efficiency due to dielectric loss. As shown in Fig. 13, the simulated efficiency of the proposed antenna with AMC structure is from 0.72 to 0.84 in the operating band. The measured efficiency is from 0.61 to 0.74. In practical applications, the dielectric loss could be mitigated by using low loss substrates.

It should be noted that in some other on-board applications, the proposed antenna could be mounted on vehicles without the AMC structure. For example, the proposed antenna can be mounted in drones to server as an offshore base station. Because the drones are covered by plastic surface, mounting on drones would not affect the antenna performance. Considering the weather of marine, the low wind drag property of the proposed antenna is quite useful and significant.

V. Conclusion

In this communication, a compact ODPA is proposed in a saber-like structure for reducing the cross section area in low wind drag applications. The HP is achieved from a thin cavity. A folded slot is directly cut on the cavity for VP. Compared with the work in [30], the VP is provided from a different mode, i.e., the slot mode instead of the monopole mode but with improvement wind drag property, i.e., 28.5% reduction, which is quite important for high-speed on-broad application. To achieve the benefit in smaller wind drag, we have paid the price of larger gain variation, such as 0.81 dB for VP. The measured bandwidth of the proposed antenna satisfies the requirement in 2.4 GHz WLAN application and the measured isolation is lower than −20 dB in the desired band. In conclusion, the proposed antenna is with potential in high-speed and low wind drag on-board communication applications.

References

[1] O. Jo, J.-J. Kim, J. Yoon, D. Choi, and W. Hong, "Exploitation of dual-polarization diversity for 5G millimeter-wave MIMO beamforming systems," *IEEE Trans. Antennas Propag.*, vol. 65, no. 12, pp. 6646–6655, Dec. 2017.

[2] P. V. Prasannakumar, M. A. Elmansouri, and D. S. Filipovic, "Wideband decoupling techniques for dual-polarized bi-static simultaneous transmit and receive antenna subsystem," *IEEE Trans. Antennas Propag.*, vol. 65, no. 10, pp. 4991–5001, Oct. 2017.

[3] Y. Li, Z. Zhang, W. Chen, Z. Feng, and M. F. Iskander, "A dual-polarization slot antenna using a compact CPW feeding structure," *IEEE Antennas Wireless Propag. Lett.*, vol. 9, pp. 191–194, 2010.
[4] C. Deng, Y. Li, Z. Zhang, and Z. Feng, "A wideband high-isolated dual-polarized patch antenna using two different balun feedings," *IEEE Antennas Wireless Propag. Lett.*, vol. 13, pp. 1617–1620, 2014.
[5] R. J. Bolt *et al.*, "Characterization of a dual-polarized connected-dipole array for Ku-band mobile terminals," *IEEE Trans. Antennas Propag.*, vol. 64, no. 2, pp. 591–598, Feb. 2016.
[6] R. D. Bari, T. Brown, S. Gao, M. Notter, D. Hall, and C. Underwood, "Dual-polarized printed S-band radar array antenna for spacecraft applications," *IEEE Antennas Wireless Propag. Lett.*, vol. 10, pp. 987–990, 2011.
[7] W. Duan, X. Y. Zhang, Y.-M. Pan, J.-X. Xu, and Q. Xue, "Dual-polarized filtering antenna with high selectivity and low cross polarization," *IEEE Trans. Antennas Propag.*, vol. 64, no. 10, pp. 4188–4196, Oct. 2016.
[8] C.-X. Mao, S. Gao, Y. Wang, F. Qin, and Q.-X. Chu, "Multimode resonator-fed dual-polarized antenna array with enhanced bandwidth and selectivity," *IEEE Trans. Antennas Propag.*, vol. 63, no. 12, pp. 5492–5499, Dec. 2015.
[9] V. Ravindra, P. R. Akbar, M. Zhang, J. Hirokawa, H. Saito, and A. Oyama, "A dual-polarization *X*-band traveling-wave antenna panel for small-satellite synthetic aperture radar," *IEEE Trans. Antennas Propag.*, vol. 65, no. 5, pp. 2144–2156, May 2017.
[10] H. Wen, Y. Qi, Z. Weng, F. Li, and J. Fan, "A multiband dual-polarized omnidirectional antenna for 2G/3G/LTE applications," *IEEE Antennas Wireless Propag. Lett.*, vol. 17, no. 2, pp. 180–183, Feb. 2018.
[11] X. Quan and R. Li, "A broadband dual-polarized omnidirectional antenna for base stations," *IEEE Trans. Antennas Propag.*, vol. 61, no. 2, pp. 943–947, Feb. 2013.
[12] E. A. Soliman, M. S. Ibrahim, and A. K. Abdelmageed, "Dual-polarized omnidirectional planar slot antenna for WLAN applications," *IEEE Trans. Antennas Propag.*, vol. 53, no. 9, pp. 3093–3097, Sep. 2005.
[13] J. Wang, L. Zhao, Z.-C. Hao, and J.-M. Jin, "A wideband dual-polarized omnidirectional antenna for base station/WLAN," *IEEE Trans. Antennas Propag.*, vol. 66, no. 1, pp. 81–87, Jan. 2018.
[14] X. Zhao, B. N. Tian, S. P. Yeo, and L. C. Ong, "Wideband segmented loop antenna with dual-polarized omnidirectional patterns for mobile platforms," *IEEE Trans. Antennas Propag.*, vol. 65, no. 2, pp. 883–886, Feb. 2018.
[15] Y. Fan, X. Liu, B. Liu, and R. Li, "A broadband dual-polarized omnidirectional antenna based on orthogonal dipoles," *IEEE Antennas Wireless Propag. Lett.*, vol. 15, pp. 1257–1260, 2016.
[16] X.-W. Dai, Z.-Y. Wang, C.-H. Liang, X. Chen, and L.-T. Wang, "Multiband and dual-polarized omnidirectional antenna for 2G/3G/LTE application," *IEEE Antennas Wireless Propag. Lett.*, vol. 12, pp. 1492–1495, 2013.
[17] H. Huang, Y. Liu, and S. Gong, "Broadband dual-polarized omnidirectional antenna for 2G/3G/LTE/WiFi applications," *IEEE Antennas Wireless Propag. Lett.*, vol. 15, pp. 576–579, 2016.
[18] D. Guo, K. He, Y. Zhang, and M. Song, "A multiband dual-polarized omnidirectional antenna for indoor wireless communication systems," *IEEE Antennas Wireless Propag. Lett.*, vol. 16, pp. 290–293, 2017.
[19] J. Wang, Z. Shen, and L. Zhao, "Wideband dual-polarized antenna for spectrum monitoring systems," *IEEE Antennas Wireless Propag. Lett.*, vol. 16, pp. 2236–2239, 2017.
[20] L. F. Zou, D. Abbott, and C. Fumeaux, "Omnidirectional cylindrical dielectric resonator antenna with dual polarization," *IEEE Antennas Wireless Propag. Lett.*, vol. 11, pp. 515–518, 2012.
[21] C. Deng, P. Li, and W. Cao, "A high-isolation dual-polarization patch antenna with omnidirectional radiation patterns," *IEEE Antennas Wireless Propag. Lett.*, vol. 11, pp. 1273–1276, 2012.
[22] Y. Liu, X. Li, L. Yang, and Y. Liu, "A dual-polarized dual-band antenna with Omni-directional radiation patterns," *IEEE Trans. Antennas Propag.*, vol. 65, no. 8, pp. 4259–4262, Aug. 2017.
[23] J. Wu, S. Yang, Y. Chen, S. Qu, and Z. Nie, "A low profile dual-polarized wideband omnidirectional antenna based on AMC reflector," *IEEE Trans. Antennas Propag.*, vol. 65, no. 1, pp. 368–374, Jan. 2017.
[24] J. Lin, Z. Qian, W. Cao, S. Shi, Q. Wang, and W. Zhong, "A low-profile dual-band dual-mode and dual-polarized antenna based on AMC," *IEEE Antennas Wireless Propag. Lett.*, vol. 16, pp. 2473–2476, 2017.
[25] D. V. Navarro-Méndez *et al.*, "Wideband double monopole for mobile, WLAN, and C2C services in vehicular applications," *IEEE Antennas Wireless Propag. Lett.*, vol. 16, pp. 16–19, 2017.
[26] Y. Li, Z. Zhang, J. Zheng, and Z. Feng, "Dual-polarised monopole-slot co-located MIMO antenna for small-volume terminals, " *Electron. Lett.*, vol. 47, no. 23, pp. 1259–1260, Nov. 2011.
[27] Y. Li, Z. Zhang, J. Zheng, and Z. Feng, "Design of dual-polarized monopole-slot antenna with small volume and high isolation," *IEEE Trans. Antennas Propag.*, vol. 60, no. 5, pp. 2511–2514, May 2012.
[28] Y. Li, Z. Zhang, J. Zheng, and Z. Feng, "Compact azimuthal omnidirectional dual-polarized antenna using highly isolated colocated slots," *IEEE Trans. Antennas Propag.*, vol. 60, no. 9, pp. 4037–4045, Sep. 2012.
[29] Y. Li, Z. Zhang, Z. Feng, and M. F. Iskander, "Design of omnidirectional dual-polarized antenna in slender and low-profile column," *IEEE Trans. Antennas Propag.*, vol. 62, no. 4, pp. 2323–2326, Apr. 2014.
[30] P. Liu, Y. Li, Z. Zhang, and Z. Feng, "Omnidirectional dual-polarized antenna with sabre-like structure," *IEEE Trans. Antennas Propag.*, vol. 65, no. 6, pp. 3221–3225, Jun. 2017.
[31] LSR Laird Business. (2015). *Integrated 802.11 b/g/n WLAN Module, TiWi-C-W Module Datasheet*. [Online]. Available: https://www.lsr.com/downloads/products/330-0129.pdf
[32] G. K. Batchelor, *An Introduction to Fluid Dynamics*. Cambridge, U.K.: Cambridge Univ. Press, 1967.
[33] A. Presse and A.-C. Taror, "Circuit model of a double-layer artificial magnetic conductor," *IEEE Antennas Wireless Propag. Lett.*, vol. 15, pp. 1061–1064, 2016.